Table III. The Two Sets of Solutions Obtained from the Nonlinear Sets of Equations in Eqs 5 and 6[a]

	solution 1		solution 2	
	$n = 3$	$n = 4$	$n = 3$	$n = 4$
$I_{residue}$	3.1	6.5	8.2	11.8
I_{carbon}	26	26	15.5	15.5
k	0.105	0.105	0.29	0.29

[a] Solution 1 is more consistent with other experimental data. I are given in arbitrary intensity units.

peaks for the multilayers than are observed. Relative to the intensity scattered by 20 nm of carbon, the first solution gives $I_{residue}$ ($n = 3$) $\approx 0.12I_{carbon}$, $I_{residue}$ ($n = 4$) $\approx 0.25I_{carbon}$, and $k \approx 0.1I_{carbon}$ (with $I_{carbon} \approx 26$ intensity units). The second solution gives $I_{residue}$ ($n = 3$) $\approx 0.53I_{carbon}$, $I_{residue}$ ($n = 4$) $\approx 0.76I_{carbon}$, $k \approx 0.29I_{carbon}$ (with $I_{carbon} \approx 15.5$ intensity units).

The first solution set implies that the thickness of the residue layer on the carbon is equivalent to ~2.5 and ~5 nm of carbon in the $n = 3$ and $n = 4$ materials, respectively. The thickness of the residue on each side of the oxide sheets is ~0.25 nm, about one or two monolayers of carbon. Coarse estimates, based on figures for typical dispersion concentrations and volumes, give figures for the residue ranging from 1 to 100 nm (assuming all dispersed solids remain behind). It is no surprise that the two specimens have different residue thicknesses, since concentration and droplet volume were not controlled between samples. It is also no surprise that the calculations indicate that there is more residue on the $n = 4$ sample. Micrographs of this specimen showed more evidence of "drying marks" than the $n = 3$ specimen (compare parts a and b of Figure 4).

The analysis here implies that most of the residue is dispersed over the carbon, presumably through diffusion of breakdown products of the surfactant. Thus, in the experiment carried out here, the residue thickness is not a reliable indicator of the amount of surfactant originally associated with each face of the oxide sheets.

Summary

In this paper, the synthesis and exfoliation of layered perovskites was described together with a new imaging technique for characterizing the extent of the exfoliation. Oxide layer thickness is deduced from the intensity scattered into a high-angle annular detector in a scanning transmission electron microscope. The advantages of the technique over shadowing methods are that it is relatively insensitive to sheet buckling, it measures the thickness at all points on the sheet rather than only at the edge, and thickness distributions can be obtained directly from the intensity histogram of a single image.

The high-angle annular detector intensity data show that $H[Ca_2Na_{n-3}Nb_nO_{3n+1}]$ ($n = 3, 5$) can be exfoliated to the level of single sheets by preintercalation of a polyether amine surfactant. The fraction of monolayers observed in exfoliated samples varied with n. About 80% of the $n = 3$ sheets observed were monolayers. However, only about 50% of the $n = 4$ sheet area was completely exfoliated and less than ~10% of the $n = 5$ sheets were true monolayers. Analysis of intensity histograms reveals small deviations from rigorously quantized intensity steps. This can be explained by the presence, on all exposed surfaces, of residual carbonaceous material, presumably originating from the breakdown of surfactant molecules when the specimen was baked.

Defect Level Identification in $CuInSe_2$ from Photoluminescence Studies

Geula Dagan,[†] F. Abou-Elfotouh,[‡] D. J. Dunlavy,[‡] R. J. Matson,[‡] and David Cahen*[,†]

The Weizmann Institute of Science, Rehovot, Israel 76100, and Solar Energy Research Institute, Golden, Colorado 80401

Received November 27, 1989

By correlating photoluminescence data with the electronic properties, stoichiometry, and chemical diffusion coefficients (of Cu) for a number of single-crystal samples, we arrive at a chemically and physically consistent interpretation of luminescent transitions in $CuInSe_2$. This interpretation involves point defect chemical assignments to the electron energy levels that are involved in these transitions. Thus the copper vacancy, V_{Cu}, is identified as a defect that is mainly responsible for Cu diffusion in this material. The electrochemical potential of the electron involved in the $V_{Cu}^{x} + e^{-} = V_{Cu}'$ reaction is found to be ca. 40 meV above the valence band.

Introduction

In the course of investigations on electronic effects of ion migration in I–III–VI_2 type semiconductors,[1] it became desirable to try to identify the chemical nature of dominant native defects in the $CuInSe_2$ samples that were studied. Results from a number of different experiments point to Cu as the most mobile species in $CuInSe_2$.[1-5] The most obvious diffusion pathways for Cu are those that involve vacancies, V_{Cu}, and those that involve interstitials, Cu_i. In both cases the antisite defect, Cu_{In}, could be involved as

[†] The Weizmann Institute of Science.
[‡] Solar Energy Research Institute.
* Author for correspondence.

(1) Soltz, D.; Dagan, G.; Cahen, D. *Solid State Ionics* **1988**, *28-30*, 1105.
(2) Tell, B.; Wagner, S.; Kasper, H. M. *J. Electrochem. Soc.* **1977**, *124*, 536. Kasper, H. M.; Tell, B.; Wagner, S. U.S. Patent 4,115,633, 1978.
(3) Becker, K. D.; Wagner, S. *Phys. Rev.* **1983**, *B27*, 5240.
(4) Kleinfeld, M.; Wiemhöfer, H. D. *Ber. Bunsen-Ges. Phys. Chem.* **1986**, *90*, 711.
(5) Kleinfeld, M.; Wiemhöfer, H. D. *Solid State Ionics* **1988**, *28-30*, 1111.

0897-4756/90/2802-0286$02.50/0

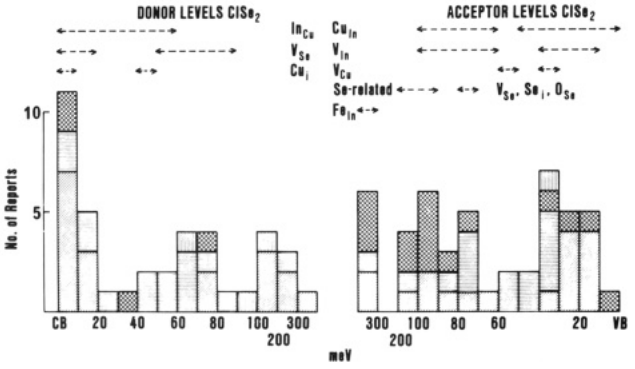

Figure 1. Histogram of reported defect levels for $CuInSe_2$. Single-crystal data are shown in the lower parts of the bars, if reported (diagonally hatched, electrical measurements; horizontally hatched, optical data); thin-film data appear above these (cross hatched, from electrical measurements; vertically hatched, from optical data). Reported (suggested) identifications of levels are indicated. Note the change in energy scale beyond 100 meV from the conduction band (CB) minimum and the valence band (VB) maximum. The middle bars refer to any level beyond 300 meV from the conduction and valence bands.

well. A first step in trying to distinguish between these diffusion mechanisms is to find a way to identify and estimate comparatively concentrations of the native defects involved in these mechanisms.

Notwithstanding the fact that the defect chemistry of $CuInSe_2$ and related compounds has been the subject of many studies and of several reviews,[6-8] considerable differences of opinion remain between interpretations made by different research groups. On the basis of literature data for both single-crystal and thin-film polycrystalline samples, we illustrate this situation in Figure 1, by way of a histogram. Several reasons exist for this situation: EPR has not been of great use in studying the native defects in $CuInSe_2$;[6] "classical" Brouwer diagrams have been proposed but not experimentally verified for $CuInX_2$ (X = S, Se);[6,9,10] experiments have often been carried out in which samples have been prepared or changed under conditions that are not controlled because of the ternary nature of the material. This makes interpretation of results of annealing/doping studies difficult at times.[11] Among the techniques that have been used for defect chemical analyses, luminescence ones, be it photo- or cathodoluminescence, appear to be among the most useful. Table I summarizes numerical estimates of donor and acceptor ionization energies, based mostly on results from luminescence studies and the defect chemical interpretation of the nature of the donor or acceptor, as offered by the original authors. Earlier compilations of this type have been presented.[12-14]

These interpretations are based in part on results from (not always controlled) annealing studies, in part on analogies to other I–III–VI_2 compounds,[15] and in part on correlations with stoichiometries derived from chemical analyses.[7] In some cases additional input has been based on theoretical estimates (that have not yet been verified experimentally) of the formation enthalpies of (neutral) defects. These estimates[16] were arrived at by extending the calculations of van Vechten for elemental and binary compound semiconductors, based on the dielectric, two-band model of semiconductors.[17] The relevant values for $CuInSe_2$ are Se_i (22.4 eV), In_i (9.1 eV), Cu_i (4.4 eV); V_{Se} (2.6 eV), V_{In} (2.8 eV), V_{Cu} (2.9 eV); In_{Cu} (1.4 eV), Cu_{In} (1.5 eV). Accordingly one expects, to a first approximation and within the limitations of this model, that antisite defects will dominate and that vacancies will be more probable than interstitials. We note though, that the model ignores steric and lattice stabilization effects. The latter can be expected to increase the energetic cost of V_{Se} formation except near the surface and to a lesser extent that of V_{In} as compared to V_{Cu} formation [cf. ref 18].

From Table I it is clear that assignments can differ significantly if only luminescence data are used to arrive at them. By also considering other types of information,

Table I. Literature Values for Donor and Acceptor Ionization Energies (in meV) Obtained from Luminescence Measurements on Single Crystals of $CuInSe_2$[a]

type	donor levels	acceptor levels	ref
n, p	70 (V_{Se})	40 (V_{Cu})	19
p	65 (V_{Se})	85 (V_{Cu})	20
n, p	60 (V_{Se}), 80 (V_{Se})[b]	40 (V_{Cu}), 80 (Se_i?)	15
p	70 (V_{Se})	40 (Cu_{In}), 80 (V_{In})	21
n	10 (V_{Se})	33 (V_{In})	12
n	35 (In_{Cu})	45 (V_{Cu}), 130 (O_{Se})	22
p	55 (Cu_i)	30 (Cu_{In}), 85 (V_{In}), 130 (O_{Se})	22
n, p	45 (In_{Cu}), 55 (Cu_i)	35 (V_{Cu}), 70 (Se_i)	23
n, p	80 (In_i), 115 (V_{Se})	30 (V_{In}), 60 (Cu_{In})	23
n	10–20 (In_{Cu}), 70 (V_{Se}), 200 (In_i)	40 (V_{Cu})	8
p	70 (V_{Se})	30 (Cu_{In}), 90 (V_{In})	8
p		89–130 (Se_i), 300–330 (V_{In})	14
n, p	40 (V_{Se}^{x}), 70 ($V_{Se}^{\bullet}$)[c]	40 (Cu_{In}''), 80 (Cu_{In}')[c]	13

[a] The defect chemical interpretation of donors and acceptors, as given by the original authors is in brackets. [b] These two levels are interpreted as being due to two different charge states, i.e., V_{Se}^{x} and $V_{Se}^{\bullet}$, or to (at least one) complex with another impurity. [c] No direct evidence is given for these charge state assignments. The original notation has been corrected to conform to the convention that the label of a defect level corresponds to the state of the defect with electron, and it has been transcribed into Kröger–Vink notation.

(6) von Bardeleben, H. J. *Sol. Cells* **1986**, *16*, 381. Cf.: Schwab, C. *Jpn. J. Appl. Phys.* **1980**, *19, Suppl. 19-3*, 59, for EPR results on $CuGaS_2$.
(7) Cahen, D. In *Ternary and Multinary Compounds*; Deb, S. K., and Zunger, Z., Eds.; Materials Research Society: Pittsburgh, 1987; pp 433–442.
(8) Rincon, C.; Wasim, S. M. In ref 7, pp 443–452.
(9) Kröger, F. A. In *Mater. Res. Soc. Symp. Proc.* **1983**, *14*, 207–224.
(10) Verheijen, A. W. Ph.D. Thesis, Catholic University of Nijmegen, The Netherlands, 1979, pp 105–121.
(11) Binsma, J. J. M. *J. Phys. Chem. Solids* **1983**, *44*, 237.
(12) Rincon, C.; Gonzalez, J.; Sanchez-Perez, G. *J. Appl. Phys.* **1983**, *54*, 6634.
(13) Sites, J. R.; Hollingsworth, R. E. *Sol. Cells* **1987**, *21*, 379.
(14) Chang, B. H.; Choi, I. H.; Park, J. D.; Irie, T. *J. Korean Phys. Soc.* **1988**, *21*, 177.
(15) (a) Masse, G.; Redjai, E. *J. Appl. Phys.* **1984**, *56*, 1154; *J. Phys. Chem. Solids* **1986**, *47*, 99. (b) Masse, G. *J. Phys. Chem. Solids* **1984**, *45*, 1091.
(16) (a) Neumann, H. In *Verbindungshalbleiter*; Unger, K., Schneider, H., Eds.; Geest & Portig: Leipzig, 1986; Chapter 9, and quoted in ref 8. (b) Neumann, H. *Cryst. Res. Technol.* **1983**, *18*, 901.
(17) van Vechten, J. A. In *Handbook of Semiconductors*; Keller, S. P., Ed.; North Holland: Amsterdam, 1980; Vol. 3, Chapter 1.
(18) Cahen, D. *J. Phys. Chem. Solids* **1988**, *49*, 103.
(19) Migliorato, P.; Shay, J. L.; Kasper, H. M.; Wagner, S. *J. Appl. Phys.* **1975**, *46*, 1777.
(20) (a) Yu, P. W. *J. Appl. Phys.* **1976**, *47*, 677. (b) Yu, P. W. *Solid State Commun.* **1976**, *18*, 395.
(21) Lange, P.; Neff, H.; Fearheiley, M.; Bachmann, K. J. *J. Electrochem. Soc.* **1985**, *132*, 2281; *Phys. Rev.* **1985**, *B31*, 4074.
(22) (a) Abou-Elfotouh, F.; Dunlavy, D. J.; Cahen, D.; Noufi, R.; Kazmerski, L. L.; Bachmann, K. J. *Prog. Cryst. Growth Charact.* **1984**, *10*, 365. (b) Abou-Elfotouh, F.; Kazmerski, L. L.; Dunlavy, D. J. *Sol. Cells* **1985**, *14*, 197. (c) Abou-Elfotouh, F.; Dunlavy, D. J.; Kazmerski, L. L.; Albin, D.; Bachmann, K. J.; Menner, R. *J. Vac. Sci. Technol.* **1988**, *A6*, 1515.
(23) Abou-Elfotouh, F.; Alkuhaimi, S.; Moustafa, R.; Dunlavy, D. J.; Kazmerski, L. L. In *Conf. Rec. 19th IEEE PV Spec. Conf.—1987*; IEEE: New York 1987; pp 770–774. Abou-Elfotouh, F.; Kazmerski, L. L.; Coutts, T. J.; Dunlavy, D. J.; Almassari, M.; Chaudhuri, S.; Birkmire, R. W. *Conf. Rec. 20th IEEE PV Spec. Conf.—1988*; IEEE: New York, 1988, pp 1520—1524.

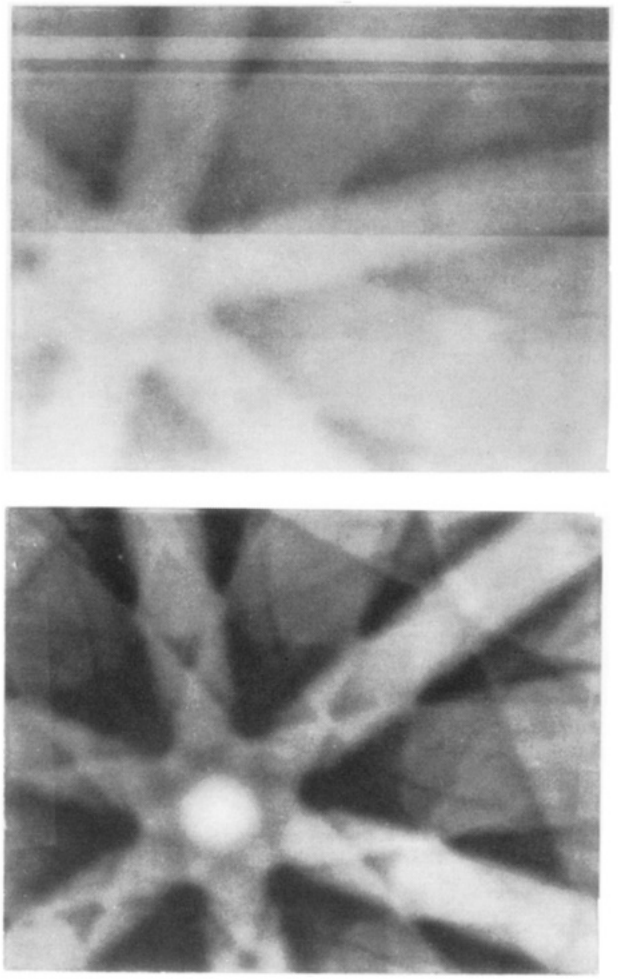

Figure 2. Electron channeling patterns of surfaces of sample E after final mechanical polish with (A) 1.0 μm or (B) 0.05 μm Al_2O_3, and chemical etch. For further details, see text.

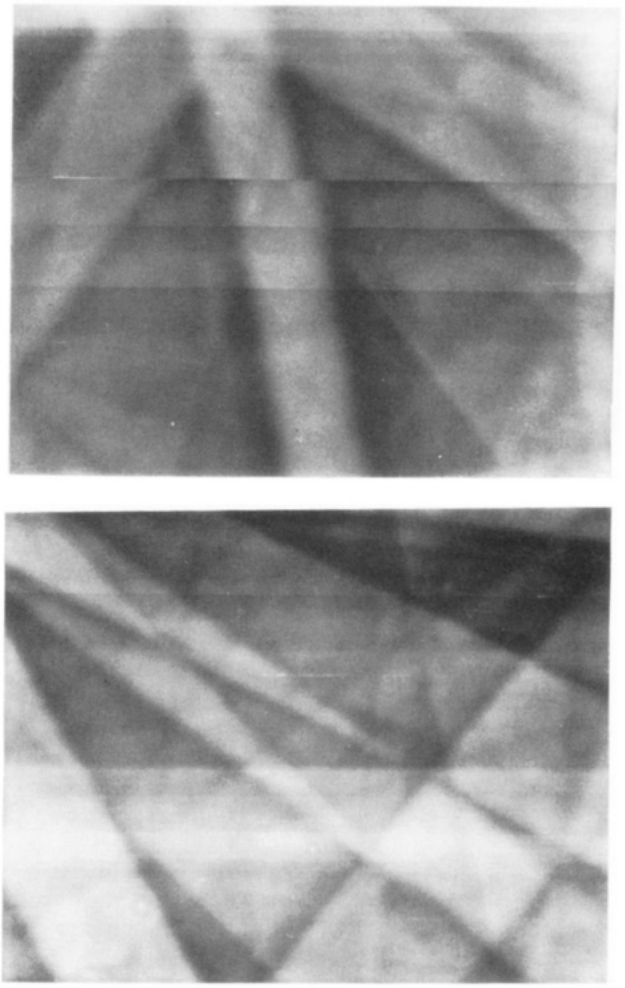

Figure 3. As in Figure 2, but for sample B, (A) after cleaving in air and (B) after final mechanical polish with 0.05 μm Al_2O_3 and chemical etch.

uncertainties in assignments can be reduced. One type of additional information that we mentioned earlier is the sample's stoichiometry. The problem is that changes in concentrations that are significant for luminescent and electronic properties can be well below the detection limits of elemental analyses. Therefore, in the following such data will be used on a limited basis, specifically by combining them with data for the chemical diffusion coefficients and with electronic parameters. In addition we followed the effects of evaporating thin strips of Cu^0, In^0, and Se^0 that were spatially separated on one and the same sample. Finally we note that in a series of separate experiments we found 10–1000-fold changes in the chemical diffusion coefficient when extra Cu was introduced (decrease) or when Cu was extracted (increase) from single-crystal samples.[24]

Experimental Section

All the crystals of $CuInSe_2$ that were used were p-type. They were obtained from three different sources. Samples B, D, and F were grown by Bachmann and co-workers at North Carolina State University by directional solidification of nearly stoichiometric melts under a Se pressure of 10^3 Pa.[25] Samples C were grown by Haupt and Hess (and obtained via the Institute for Physical Electronics, University of Stuttgart). They were prepared by the vertical Bridgman method by cooling the prereacted melt from 1020 to 750 °C at 2 °C/h and from 750 °C downward at 10 °C/h.[26]

Samples E were grown by Endo and co-workers at the Science University of Tokyo by melting of the elements in an evacuated quartz ampule followed by directional freezing. Details on the growth temperature program are given in ref 27.

All samples were polished with Al_2O_3 powder, using successively smaller Al_2O_3 particle sizes, down to 0.05 μm. The polished samples were then etched for 15 s in 0.5% (v/v) Br_2/CH_3OH solution. This procedure was adopted to minimize the possibility of contributions to the photoluminescence (PL) signal from a surface layer that is damaged and/or contaminated. For $CuInSe_2$ such contributions can be even more significant than for other semiconductors because of the material's large optical absorption coefficient ($>10^5$ cm^{-1} at 647.1 nm, the excitation wavelength used by us for the PL experiments), resulting in a correspondingly small optical absorption length. The effects of these surface treatments were followed by electron channeling (Figures 2 and 3).

An electron channeling pattern (ECP) results from rocking a collimated beam of electrons (in the scanning electron microscope, SEM) about a point on the surface of the sample and recording the variation in the intensity of backscattered electrons due to their (in)ability to channel (i.e., be diffracted).[28] The channeling patterns were obtained by using a JEOL 35C SEM, operated at 35 kV and 250 μA in the secondary electron imaging mode. (The high currents that were used explain the electrical charging that is evident in the patterns.) The sampling depth is between 50

(24) Dagan, G.; Cahen, D. To be published.
(25) Bachmann, K. J.; Fearheiley, M.; Shing, T. H.; Tran, N. *Appl. Phys. Lett.* **1984**, *44*, 407.
(26) Haupt, H.; Hess, K. In *Ternary Compounds. Inst. Phys. Conf. Ser.* **1977**, *35*, 5.
(27) Endo, S.; Irie, T.; Nakanishi, H. *Sol. Cells* **1986**, *16*, 1.
(28) Joy, D. C.; Newbury, D. E.; Davidson, D. L. *J. Appl. Phys.* **1982**, *53*, R81. Joy, D. C. *Cryst. Prop. Prep.* **1988**, *16*, 81.

Table II. Stoichiometry (Determined by EDS Analyses[a]) of $CuInSe_2$ Samples Used in This Study and Their Measured Chemical Diffusion Coefficients

sample	Cu, at. %	In, at. %	Se, at. %	diff coeff, cm^2/s
B	23.7	26.2	50.0	2.4×10^{-10}
C	24.2	25.6	50.2	1.0×10^{-9}
D	23.1	26.0	50.8	5.3×10^{-7}
E	23.7	25.2	51.0	4.9×10^{-8}
F	22.6	26.6	50.8	8.1×10^{-7}

[a] Estimated accuracies are ca. 0.2 at. % (Cu, In) and 0.4 at. % (Se). Differences between 100 at. % and the sum of the percentages are due to rounding off to one decimal place.

and 100 nm, up to twice the extinction distance, which we calculated to be ca. 35 nm in the [112] direction under our experimental conditions. Thus, because the contrast of an ECP comes from a region that is only a few tens of nanometers deep, it will be best if the surface is clean, free of oxides, and not damaged (free of disorder and strain). Indeed, our use of ECPs came about because of observed qualitative differences in channeling patterns between cleaved and mechanically polished surfaces.

In the case of the E crystals whose patterns are shown in Figure 2, a major pole could be distinguished, the [112] direction. This suggests that the crystals were cut perpendicular to the growth direction,[27] as this plane is known, from descriptive mineralogy, to be the preferred growth plane of chalcopyrite, $CuFeS_2$, and roquesite, $CuInS_2$.[29] Figure 2 shows the improvement in the crystalline quality of the surface following a finer mechanical polish. Figure 3 shows channeling patterns of a sample of type B. The quality of the pattern from a polished and etched sample is comparable to that of the surface of a sample that was cleaved (ex situ). The latter's pattern suggests a major pole in the [012] direction. (Chalcopyrite cleaves preferably on the {011} plane.[29])

Separated strips of Cu, In, and Se were evaporated on the polished and etched surfaces of samples of types E and F. The sample plus strips were then heated at 200 °C in the vacuum of the SEM, for ca. 30 min. The strips were generally ca. 1 × 3 mm and separated by ca. 1 mm. After being heated, the Se strip mostly disappeared, presumably because of sublimation. The remainder of the Cu and In strips were removed by dipping in "orostrip" etchant (which removed the In), by light polishing (0.3 and 0.05 μm Al_2O_3) and subsequent reetching. Junction electron-beam-induced current (JEBIC) measurements[30] were performed on cleaved samples with a large area Au back contact and a (ca. 0.25-mm^2 area) W needlepoint contact to the surface, onto which the strips had been deposited. The needle was positioned onto a strip of Ag that was painted along this surface, thus allowing us to view the different regions under this surface without the need to reposition the needle. The JEBIC measurements showed shallow junctions under the areas where the Cu and In strips had been deposited, but not under the area of the Se strip. Cu and In are known to be capable of making $CuInSe_2$ less p-type or even to type convert it, after in-diffusion.[31,32]

Photoluminscence spectra were obtained at temperatures between 7.4 and 80 K, by using the 647.1-nm emission line from a Kr laser with incident intensities between 5 and 40 mW. The laser beam was focused on a 0.2-mm-diameter spot on the sample. This allowed us to excite areas that had been influenced by one of the extra metal layers, deposited on the surface (see above). The emission spectra were analyzed by a SPEX Model 1680 double-grating monochromator (~0.2-nm resolution, i.e., ca. 0.2 meV in the spectral region of interest here). The signal was detected by a Ge detector. Several samples of each type were measured, and on each sample several spots were used to check for possible sample inhomogeneities. Samples E and F were found to be the most homogeneous. Still differences between spectra from different spots on the samples were much less than those between spectra from different sample types and referred mostly to variations in relative intensities between peaks and shoulders and not to the absence or presence of spectral features.

Table III. Electronic Parameters of Samples Used in This Study and Their Measured Chemical Diffusion Coefficients

sample	resistivity, Ω cm	mobility, $cm^2/V \cdot s$	N_a, cm^{-3}	diff coeff, cm^2/s
B	0.9	30	2.2×10^{17}	2.4×10^{-10}
C	0.7	15	6.5×10^{17}	1.0×10^{-9}
D	2.1	6	5.0×10^{17}	5.3×10^{-7}
E	15	30	1.4×10^{16}	4.9×10^{-8}
F	4500	10	1.5×10^{14}	8.1×10^{-7}

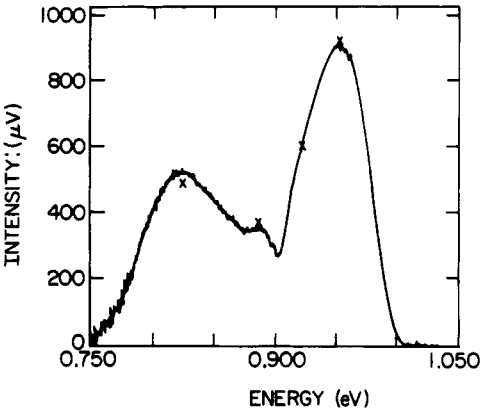

Figure 4. Photoluminescence spectrum of p-$CuInSe_2$ single crystal (sample B) at 7.8 K and 25-mW excitation intensity; two scans.

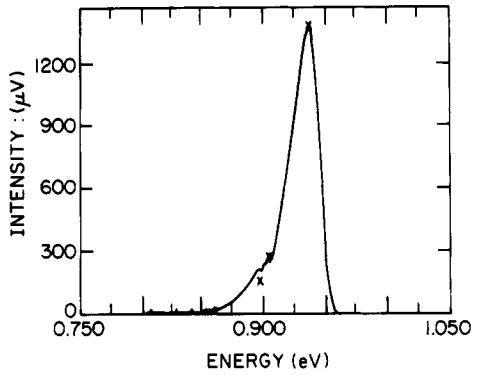

Figure 5. Photoluminescence spectrum of p-$CuInSe_2$ single crystal (sample C) at 7.4 K and 10-mW excitation intensity; two scans and double the slit width of the spectrum shown in Figure 4.

Stoichiometries of the samples were determined by energy dispersive X-ray fluorescence spectroscopy (EDS), in a Philips Model 515 SEM, equipped with a TRACOR EDS system and with a CAMECA MBX electron microscope using wavelength-dispersive X-ray fluorescence spectroscopy (WDS). The electron beam voltage was mostly 20 kV. The precision of the analyses stems from multiple sampling. Their accuracy is determined by a reference crystal, the composition of which was measured by multiple chemical and atomic absorption analyses (WDS) or by WDS (for the EDS analyses). The composition of the reference crystal is checked before each run of analyses.

Electrical measurements were done using a four-contact van der Pauw configuration and, for Hall effect measurements, a field of 20 kG. Chemical diffusion coefficients were determined by using the point electrode configuration of current decay measurements developed by Rickert and Wiemhöfer[33] and applied earlier to $CuInS_2$ and $CuInSe_2$.[1,4,5] Tables II and III summarize the stoichiometries, electrical properties, and chemical diffusion

(29) Mason, B.; Berry, L. G. *Elements of Mineralogy*, Freeman: San Francisco, 1968.
(30) Matson, R. J. *Scanning Microsc.* **1988**, *2*, 121.
(31) Tomlinson, R. D.; Elliot, E.; Parkes, J.; Hampshire, M. J. *Appl. Phys. Lett.* **1975**, *26*, 383.
(32) Parkes, J.; Tomlinson, R. D.; Hampshire, M. J. *J. Cryst. Growth* **1973**, *20*, 315.
(33) Rickert, H.; Wiemhöfer, H. D. *Solid State Ionics* **1983**, *11*, 257.

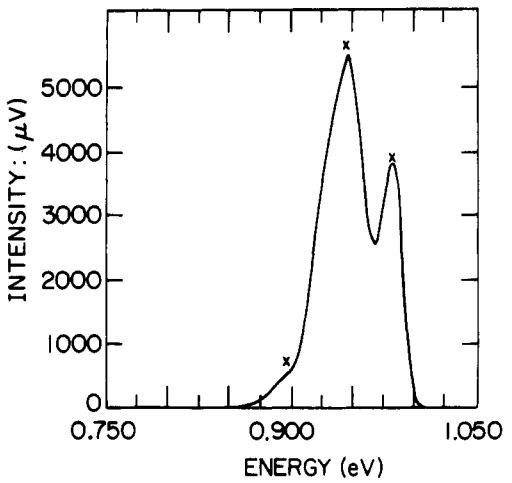

Figure 6. Photoluminescence spectrum of the cleaved surface of a p-$CuInSe_2$ single crystal (sample D) at 7.8 K and 25-mW excitation intensity; one scan; slit width as in Figure 4.

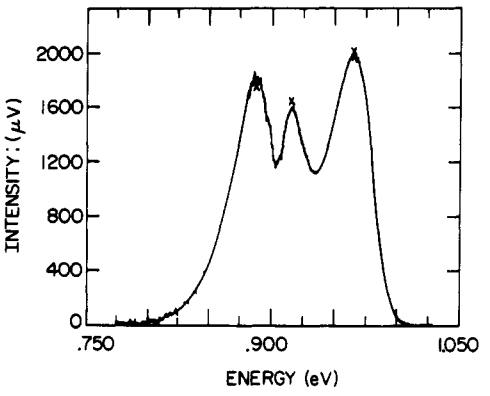

Figure 7. Photoluminescence spectrum of p-$CuInSe_2$ single crystal (sample E) at 7.8 K and 25-mW excitation intensity; two scans; slit width as in Figure 4.

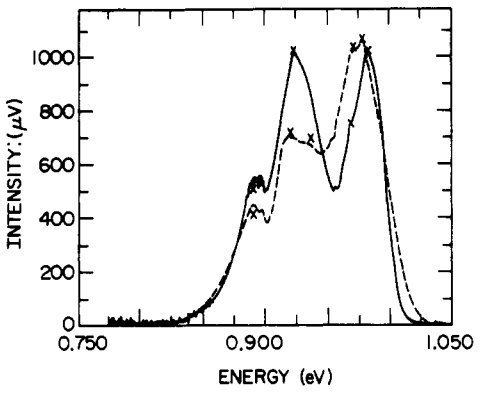

Figure 8. Photoluminescence spectra of p-$CuInSe_2$ single crystal (sample F) at 7.8 K (—) and at 40 K (– – –, smoothed), using 25-mW excitation intensity; two scans; three-fifths the slit width of the spectrum shown in Figure 4 was used. For the 40 K spectrum the intensity scale has been divided by 0.76.

coefficients of the samples used.

Results

Figures 4–9 show representative, 7–8 K photoluminescence spectra of the five types of samples that were studied. The estimated positions of peaks and shoulders are indicated on the spectra by ×. At these low temperatures the band-to-band transition is not observed in these samples.

Figure 4 shows the measured photoluminescence spectrum of sample B. The main transition is at 0.953 eV. Two

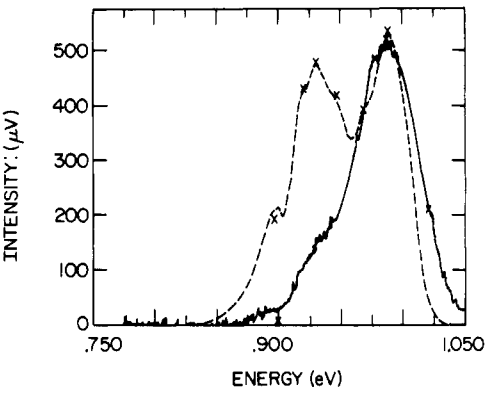

Figure 9. Photoluminescence spectra of p-$CuInSe_2$ single crystal (sample F) at 7.7 K and 40 mW (– – –, two scans, smoothed) and at 80 K and 50-mW excitation intensity (—, 3 scans); slit widths are as in Figure 8. For the 7.7 K spectrum the intensity scale has been divided by 3.2.

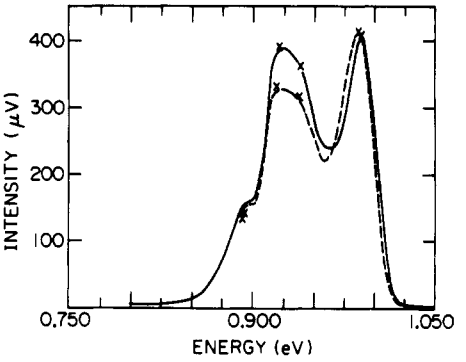

Figure 10. Photoluminescence spectra from two areas of p-$CuInSe_2$ single crystal (sample F) at 7.6 K and 10-mW excitation intensity, after thermal diffusion experiment: —, from area onto which a Cu strip was deposited; – – –, from area that was well removed from those onto which Cu, In, or Se were deposited. The slit widths are as in Figure 8; two scans; smoothed spectra.

shoulders (at 0.92 and 0.89 eV) and a broad peak at low energy (0.826 eV) are observed as well. In Figure 5 (sample C) only one dominant transition at 0.936 eV is observed. Two strong transitions were measured for sample D (Figure 6); their energies are 0.987 and 0.949 eV. A shoulder at 0.90 eV is observed as well. Three strong peaks are seen in the spectra of sample E (Figure 7), at 0.968, 0.917, and 0.888 eV. At higher temperatures (25–60 K) a peak at 0.94–0.95 eV grows in for some of the samples.

The most intensive work was done on samples from batch F, which appeared to be, together with samples E, of highest quality in terms of single crystallinity and lack of microcracks. Four dominant transitions are observed at 7.8 K (Figure 8), at 0.986, 0.971 (shoulder), 0.925, and 0.893 eV. At higher temperatures (15–60 K) two additional shoulders at 0.946 and 0.935 eV start to emerge (Figure 8). At a temperature of 40 K and higher (up to 80 K), the spectra of samples F show a decrease in the intensity for all the emissions but much less so for the one at 0.98 eV (Figure 9). Similar to what is found for samples E, the only dominant peak at 80 K is the high-energy peak (0.98 eV, in this case). This peak shifts to higher energy, and a shoulder appears at 1.02 eV (probably the band-to-band transition) as is shown in Figure 9. This shift to higher energy was observed also when samples were measured at 7.8 K after annealing at 200 °C in vacuum (cf. Figures 10 and 11).

Thermal diffusions of Cu and In were performed on samples E and F. The PL spectra were measured before and after these treatments. This was done to identify the

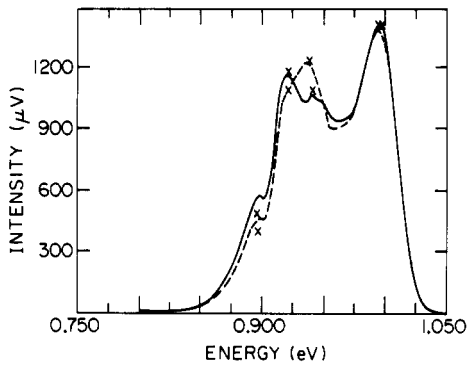

Figure 11. Photoluminescence spectra from two areas of p-$CuInSe_2$ single crystal (sample F) at 7.6 K and 40-mW excitation intensity, after thermal diffusion experiment: ---, from area onto which an In strip was deposited (intensities have been divided by 1.04); —, from area that was well removed from those onto which Cu, In, or Se were deposited. The slit widths are as in Figure 8; two scans; smoothed spectra.

elements that are involved in the point defects, whose energy levels are related to the various transitions.

The results from samples F were the cleanest. They show a decrease in the intensity of the peak at 0.92 eV and to a lesser extent that at ca. 0.95 eV, after diffusion of Cu (Figure 10). Thermal diffusion of In results in a decrease in the intensity of the transition at 0.89 eV and in some increase in the intensity of the peak at 0.95 eV (at 40-mW excitation intensity; cf. Figure 11). We did not see a clear effect at lower excitation intensity.

The intensities of the PL spectra scaled approximately with excitation power. No clear shifts in the energy positions of the peaks or the shoulders were observed as the excitation power was varied. This is not surprising because of the relatively narrow range of intensities that was accessible to us. As noted already for sample F, the effects of increasing temperature were more pronounced, with most peaks or shoulders shifting to higher energies and many of them decreasing in intensity (cf. Figures 8 and 9). These changes will be discussed below where appropriate. In the case of the higher doped E samples, the only clear effect of metal strip deposition and subsequent thermal in-diffusion was a pronounced decrease in the 0.91–0.95-eV intensity with respect to the other parts of the spectrum.

Discussion

Our ability to interpret these PL results is limited by their complexity, something that is a result of the ternary character of the material and the quality of the samples, and by the experimental limitations (lowest achievable temperature and range of excitation intensities). The main experimental variables that can assist us in interpreting the data are the dependence on sample stoichiometry, on metal in-diffusion, and on vacuum annealing and the temperature dependence. An increase in temperature is expected to lead to increases in energy of the free-to-bound, of the bound-to-bound, and of exciton-involving transitions. The last types are not expected to play a major role in our samples as they are normally encountered only in very pure materials. The intensitites of the bound-to-bound transitions will decrease, while those of the free-to-bound ones will be relatively unaffected by an increase in temperature. The bound-to-bound transitions can be widened (toward the high-energy side) by electrostatic interaction between charged defects, especially at high excitation intensities and for samples with high concentrations of defects. A simple electrostatic calculation shows that the effect can be ca. 100 meV (e.g., for samples C and D, taking the net acceptor concentration as an indication for the total one) or less than 10 meV (sample F). In our experiments we did not see clear evidence for distinct shoulders due to the electrostatic interaction. Neither did we find convincing experimental evidence for low-energy broadening of transitions due to phonon replica. On the basis of infrared data of Neumann and co-workers,[34] shifts to or shoulders at ca. 8, 23, 26, and 29 meV can be expected, well within our experimental resolution. Thus if any or both of these effects plays a role, they will probably be expressed only as broadening of peaks.

The use of hydrogenic levels as a guide, which has been attempted in the past,[12] appears to be of limited value, as at our present level of knowledge we can calculate only one acceptor level, at 45 meV above the valence band (VB) maximum, and one donor level, at ~6 meV below the conduction band (CB) minimum (this value is about half that calculated in ref 35, because there an incorrectly estimated value for the dielectric constant was used).

In the light of these remarks we will concentrate on the gross features of the spectra, relying primarily on comparison between them for their interpretation.

General Points. The high-energy band (0.98 eV), which appears in samples D and F and as a shoulder in sample E, was previously attributed to a transition due to the free electron to bound hole to acceptor (F–B).[15,19,20,22] At high temperatures or after annealing, a shift of this transition to higher energies is observed (Figures 8–11). This shift was explained by the shift of the bandgap energy to higher values.[20a] The other bands were attributed to donor–acceptor transitions (D–A).[15,19–22]

The temperature dependence of the various transitions supports these interpretations. Strong decreases in intensity were observed for all the transitions (except that at 0.98 eV) when measured at elevated temperatures (Figures 8 and 9). This temperature dependence supports the idea that the transition at 0.98 eV is free-to-bound and the emissions at lower energy are donor–acceptor (bound-to-bound).[20]

The 0.98-eV Transition. The free-to-bound emission at 0.98 eV is dominant in samples D and F (Figures 6 and 7, respectively) in which the Cu content is the lowest among the five samples that were measured. The transition at 0.98 eV does not appear in the spectrum of sample C and could be hidden under the broad 0.968-eV peak in sample E (Figures 5 and 7, respectively). The spectrum of sample B is very broad, but even if the 0.98-eV band is hidden in the large peak, clearly it does not correspond to a dominant transition.

An acceptor level was observed at about 40 meV above the valence band and attributed to Cu vacancy[15,19,20,22] or to In vacancy.[12] The first interpretation fits our results better because most of the samples that were measured have Cu/In < 1. It was also suggested[36] that V_{Cu} will be more likely than V_{In} in $CuInSe_2$ because Cu might participate only weakly in the covalent bonding (cf. also ref 2). According to this, a large concentration of vacancies of copper is expected in p-$CuInSe_2$.

The intensity of the transition at 0.98 eV (normalized to identical experimental conditions) decreases in the order D > F > E (it is not observed in samples B and C). These three samples are Cu-poor, In-rich p-type materials. The

(34) Neumann, H.; Tomlinson, R. D.; Kissinger, W.; Avgerinos, N. *Phys. Status Solidi B* **1983**, 118, K51. Neumann, H. *Sol. Cells* **1986**, *16*, 399.
(35) Irie, T.; Endo, S.; Kimura, S. *Jpn. J. Appl. Phys.* **1979**, *18*, 1303.
(36) Tell, B.; Shay, J. L.; Kasper, H. M. *J. Appl. Phys.* **1972**, *43*, 2469.

free-to-bound peak at 0.98 eV was related to the transitions CB → V_{Cu}[15,19,20] to In_{Cu} → VB,[23] and to Cu_i → VB,[23] but as it appears as a dominant transition in the Cu-poor samples (F, D) and because our samples are p-type (acceptors will dominate), the first interpretation (CB → V_{Cu}) is more likely.

The 0.89- and 0.92-eV Transitions. The donor–acceptor transitions at 0.89 and 0.92 eV are observed, at different relative intensities, in all five of the samples. The 0.92-eV transition is hidden under the (dominant) 0.935-eV one in the spectrum of samples C. It starts to appear, as a shoulder, with increasing excitation intensity. The intensities of these transitions on an absolute scale decrease in the order E > F > D > B > C (for the peak at 0.89 eV) and D > F > E > B > C (for the transition at 0.92 eV).

A donor level at about 70 meV below the conduction band was deduced by many investigators.[8,15,19-21,37,38] This defect level was attributed to a Se vacancy. Masse and Redjai[15] found two donor levels at 60 and 80 meV and assigned both to a Se vacancy. Se_i, which was suggested for the 70–80 meV acceptor level,[15b,23] is not probable because of steric and lattice stabilization considerations[18] and because of the very high formation energy (22.4 eV) that has been calculated for this point defect.

The transition at 0.92 eV is assigned to a donor–acceptor. We attribute it to the V_{Se} → V_{Cu} transition, as was also suggested before.[15,19] The decrease in the intensity of the transition at 0.92 eV after thermal diffusion of Cu into the sample (Figure 10) supports the assignment of this defect to V_{Cu}. The order of the intensity of this transition among the various samples parallels that of the transition at 0.98 eV (D > F > E). This fits the interpretation that both transitions involve the same point defect (V_{Cu} in this case).

The emission at 0.89 eV is probably due to the D–A transition from V_{Se} to the acceptor level at 80 meV above the valence band. The assignment of this level is not agreed upon. In several reports it was attributed to vacancy of In.[8,21,22,39] The decrease in the intensity of the peak at 0.89 eV after thermal diffusion of In into the material (Figure 11) supports the suggestion that this peak represents a transition to V_{In}. Significant concentrations of vacancies of In are reasonable in these samples only if the samples are highly disordered. The (calculated) low formation energy (1.4 eV) of the defects related to cation disorder, the low concentration of Cu, and the high concentrations of In, support the occurrence of In on Cu site.

Other Transitions. As the Cu concentration of sample C is almost stoichiometric (the highest among the samples that were measured) and from the low formation energy of Cu_{In}, this is a likely acceptor to be present in sample C. The most probable donors are V_{Se} and In_{Cu}. On the basis of the chemical analyses and on defect levels from the literature, the donor–acceptor emission at 0.935 eV which is the dominant transition for sample C (Figure 5) can be related to the transition V_{Se} → Cu_{In}. The emission at 0.935 eV is observed also in sample F at higher temperatures (Figures 8 and 9).

The peak at 0.945 eV, which was observed for samples B, D, and F, can be connected to the D–A transition In_{Cu} → V_{Cu}. This assignment is based on the chemical analyses (it appears in the most Cu-poor and In-rich samples), on energy levels from the literature, and on the fact that its intensity is increased by thermal diffusion of In into the material.

A transition at 0.96–0.97 eV appears as a shoulder in samples E and F. On the basis of defect levels it can be attributed to the transition In_{Cu} → Cu_{In}.

The peak at the lowest energy, 0.82 eV, is observed in sample B (Figure 4). It can be related to transition from the donor level at about 200 meV, which was found by electrical measurements[35,40] and was assigned to In_i.[8]

The PL emissions for the samples that were studied, as well as our assignments for them, are summarized in Tables IV and V.

Correlation with Chemical Diffusion Coefficients. High chemical diffusion coefficients ($\tilde{D}$) are observed for samples F and D, in which the main PL transition is at 0.98 eV (no. 1). It appears as a strong transition *only in these two samples* and is attributed to the free-to-bound transition CB → V_{Cu}. The Cu content of samples D and F is the lowest (cf. Table II), which implies a high concentration of Cu vacancies. The transition of 0.98 eV appears as a shoulder in the PL spectrum of sample E, which exhibits a moderate chemical diffusion coefficient.

Low Cu content appears also in sample B, but its main transition is no. 5 (In_{Cu} → V_{Cu}), which points out that some fraction of the Cu vacancies is occupied by the excess of In. The free-to-bound transition no. 1 is not observed. Thus, in sample B the concentration of V_{Cu} is apparently low, the diffusion through this defect is blocked, and, as can be observed in Table V, the diffusion coefficient is low.

Sample E contains vacancies of Cu and of Se as well as disorder defects (In_{Cu} and Cu_{In}). This disorder can explain the existence of some copper vacancies that are apparent from transition no. 2. Indium on Cu sites eliminates part of the Cu vacancies and can block their migration, while copper on indium sites will give rise to creation of new Cu vacancies.

In sample C only the 0.92-eV transition, from all of those in which Cu vacancies are thought to take part (transitions no. 1, 2, or 5 of Table IV), appears to be present. Therefore we conclude that the dominant defects are Cu_{In} and V_{Se},

Table IV. Summary of the Dominant PL Emissions in p-$CuInSe_2$ (Measured at 7.4–7.8 K)

no.	energy, eV	assignment[a]	obsd in samples
1	0.98	CB → V_{Cu} (A3)	F, D
2	0.92	V_{Se} → V_{Cu} (B2)	all
3	0.89	V_{Se} → V_{In} (B3,B4)	all
4	0.935	V_{Se} → Cu_{In} (B12)	F, C
5	0.95	In_{Cu} → V_{Cu} (B1)	F, D, B
6	0.96–0.97	In_{Cu} → Cu_{In}	E, F

[a] The peak nomenclature of refs 22 and 23 is given in parentheses.

Table V. Main Defects in Several p-$CuInSe_2$ Samples According to the Measured Photoluminescence Spectra (at 7.4–7.8 K) and Their Measured Chemical Diffusion Coefficients ($\tilde{D}$)[a]

sample	main transitions	main defects	$10^9\tilde{D}$, cm^2/s
F	1, 2 (at 7.8 K) 1 at (60–80 K)	V_{Cu} (a), V_{Se} (d)	810
D	1, 5	V_{Cu} (a), In_{Cu} (d)	530
E	2, 3, 6	V_{Cu} (a), V_{Se} (d), V_{In} (a) In_{Cu} (d), Cu_{In} (a)	49
C	4	Cu_{In} (a), V_{Se} (d)	1.0
B	5	V_{Cu} (a), In_{Cu} (d)	0.24

[a] a, acceptor; d, donor.

(37) Neumann, H.; Tomlinson, R. D.; Avgerinos, N.; Nowak, E. *Phys. Status Solidi A* **1983**, *75*, K199.
(38) Rincon, C.; Bellabarba, C. *Phys. Rev.* **1986**, *B33*, 7160.
(39) Von Bardeleben, H. J. *J. Appl. Phys.* **1984**, *56*, 321.
(40) Neumann, H.; Nowak, E.; Kuhn, G. *Cryst. Res. Technol.* **1981**, *16*, 1369.

with V_{Cu} as a minor species.

Conclusion

From the photoluminescence data presented here it is apparent that the important defect for diffusion is the copper vacancy. This finding confirms results from the effects of chemical treatments on $\tilde{D}_{Cu}$ in $CuInSe_2$, which we mentioned earlier, and which will be reported on and discussed in a future publication.

More complete (and firmer) interpretation of luminescence spectra of $CuInSe_2$ may become possible by wider use of metal in-diffusion experiments and Cu extraction, to control Cu content, working at lower temperatures, avoiding the use of samples with damaged surface regions, and use of wider supplies of high quality crystals.

Acknowledgment. We thank K. Bachmann (North Carolina State University), H. W. Schock (IPE, University Stuttgart), and S. Endo (Science University of Tokyo) for samples of $CuInSe_2$. This research is supported, in part, by the US-Israel Binational Science Foundation, Jerusalem, Israel, and by the Israel National Council for Research and Development with the KFA Jülich (FRG). At SERI research is supported by the US Department of Energy under Contract DE-AC02-83CH10093.

Registry No. $CuInSe_2$, 12018-95-0.

X-ray Photoelectron Spectroscopic Studies of Carbon Fiber Surfaces. 11. Differences in the Surface Chemistry and Bulk Structure of Different Carbon Fibers Based on Poly(acrylonitrile) and Pitch and Comparison with Various Graphite Samples

Yaoming Xie and Peter M. A. Sherwood*

Department of Chemistry, Kansas State University, Manhattan, Kansas 66506

Received November 28, 1989

X-ray photoelectron spectroscopy has been used to monitor the surface chemistry of untreated carbon fibers based on PAN and pitch, a pitch fiber anodically oxidized in 1 M HNO_3, and three different graphite materials. Differences were found in the core and valence-band region indicating a highly graphitic and almost unoxidized nature for untreated pitch-based fibers. The graphite samples were found to have more reactive surfaces than the pitch fibers. X-ray powder diffraction was used to study the bulk structures of these materials, and the Du Pont E-120 pitch-based fiber was found to have the most graphitic structure of all the carbon fibers examined. The anodic oxidation of the pitch fiber changed both surface and bulk structure, producing mainly one type of oxygen-containing group on the surface.

Introduction

The mechanical properties and the surface treatment of carbon fibers are both important in producing composite materials with the desired properties. These composites are now widely used, especially in the aircraft industry. We have carried out a range of studies of different carbon fiber surfaces for both PAN (polyacrylonitrile) and pitch-based carbon fibers using various surface treatments.[1-10] Our previous studies had focused on the surface chemistry, mainly measured by X-ray photoelectron spectroscopy (XPS or ESCA), an approach we and other workers (see the review in ref 9) have found to be very valuable.

In this paper we compare the surface chemistry as measured by XPS (using both core and valence band XPS) with the bulk properties as measured by powder X-ray diffraction (XRD). We discuss the two main types of carbon fiber, namely, those prepared from PAN and those prepared from pitch (both untreated and treated), and compare these fibers with three different qualities of graphite.

Experimental Section

Five different untreated carbon fiber samples were studied, two (a and b) were type II fibers based upon PAN and three (c–e) were different modulus pitch-based fibers. Sample j is the same as sample e but was examined by using Al X-rays. Sample i was surface treated by electrochemical oxidation. The three different quality graphite samples were samples f–h. Further details of the samples and sample treatment are given in Table I. The results reflect typical spectra for the samples. We have carefully studied a number of samples. In the case of the fibers we have in all our studies[1-10] carefully ensured that initially untreated and unsized samples from the original manufactures were obtained. We have also checked to ensure that there were no significant variations associated with the location of the fiber in the fiber tow. Types of fiber simliar to a–c were discussed in a previous publication,[10] and they are reported here to compare and to discuss their XRD. In this paper, these samples represented a different sample from the same type of carbon fiber.

The X-ray photoelectron (XPS or ESCA) spectra were collected on an AEI (Kratos) ES200B X-ray photoelectron spectrometer with a base pressure of about 10^{-9} Torr (except sample f where the spectra were collected on a VSW HA100 XPS instrument with

(1) Proctor, A.; Sherwood, P. M. A. *J. Electron Spectrosc.* **1982**, *27*, 39.
(2) Proctor, A.; Sherwood, P. M. A. *Carbon* **1983**, *21*, 53.
(3) Proctor, A.; Sherwood, P. M. A. *Surf. Interface Anal.* **1982**, *4*, 212.
(4) Kozlowski, C.; Sherwood, P. M. A. *J. Chem. Soc., Faraday Trans. 1* **1984**, *80*, 2099.
(5) Kozlowski, C.; Sherwood, P. M. A. *J. Chem. Soc., Faraday Trans. 1* **1985**, *81*, 2745.
(6) Harvey, J.; Kozlowski, C.; Sherwood, P. M. A. *J. Mater. Sci.* **1987**, *22*, 1585.
(7) Kozlowski, C.; Sherwood, P. M. A. *Carbon* **1986**, *24*, 357.
(8) Kozlowski, C.; Sherwood, P. M. A. *Carbon* **1987**, *25*, 751.
(9) Xie, Y.; Sherwood, P. M. A. *Appl. Spectrosc.* **1989**, *43*(7), 1153.
(10) Xie, Y.; Sherwood, P. M. A. *Chem. Mater.* **1989**, *1*, 427.

0897-4756/90/2802-0293$02.50/0